Supplementary Information

Nonv-olatile ferroelastic switching of the Verwey transition and resistivity in epitaxial Fe_3O_4/PMN-PT (011)

Ming Liu,[1*] Jason Hoffman,[2] Jing Wang,[3] Jinxing Zhang,[3*] Brittany Nelson-Cheeseman[2] and Anand Bhattacharya[1,2*]

1. Center for Nanoscale Materials, Argonne National Laboratory, Argonne, IL 60439 (USA)

2. Material Science Division, Argonne National Laboratory, Argonne, IL 60439 (USA)

3. Department of Physics, Beijing Normal University, Beijing 100875 (China)

[*] mingliu@anl.gov, jxzhang@bnu.edu.cn, anand@anl.gov

1. Growth of epitaxial Fe_3O_4 films by oxide MBE

In order to determine optimal growth conditions, single-crystalline epitaxial films of Fe_3O_4 were grown on MgO (001), $MgAl_2O_4$ (001), PMN=PT(001), and PMN-PT(011) substrates, using ozone-assisted molecular beam epitaxy (MBE). The films were characterized by *in situ* reflection high-energy electron diffraction (RHEED), x-ray diffraction and reflectivity. Prior to growth, the MgO (001) substrates were cleaned by acetone and methanol ultrasonic baths, followed by heating up to 600 °C in the MBE chamber in the presence of ozone at a pressure of $2x10^{-6}$ Torr for 10 min. This treatment removed all contaminants and surface phase of brucite $Mg(OH)_2$ that forms as atmospheric water reacts with MgO. During the growth, the substrate temperature was held at 300 °C and a flow of pure distilled ozone was delivered to the substrate while maintaining the chamber pressure at $1.0x10^{-7}$ Torr. Fe of 99.9% purity was deposited from a dual-filament Knudsen cell, which was differentially pumped so that the heated source material was exposed to a lower pressure (~ 2 x 10^{-8} Torr). The deposition rate was measured prior to film growth, using a quartz-crystal thickness monitor (QCM). The shutter of the Fe was opened to deposit a single-unit-cell layer in 180-240 s. When the deposition was complete, the sample was cooled to room temperature in ozone. The deposition rate of the source material was measured again post growth, with drift in the rates typically ~ 0.5% per hour.

Figure S1 shows x-ray diffraction patterns of iron oxide films deposited on MgO substrates under various ozone pressures, using a 4-bounce high resolution monochromator. Upon increasing the ozone pressure from 1×10^{-7} to 2×10^{-6} Torr, the *c*-axis lattice parameter reduced from 8.3808 Å to 8.3162 Å, suggesting a transition from Fe_3O_4 (a = 8.396 Å in bulk) to γ-Fe_2O_3 (a = 8.345 Å in bulk). The increasing lattice mismatch between MgO and iron oxide films of Fe_3O_4 (-0.36%) and Fe_2O_3 (-0.89%) upon increasing the oxidation state of Fe[1] may also play a role in stabilizing the magnetite phase at a lower ozone pressure of 1×10^{-7} Torr.

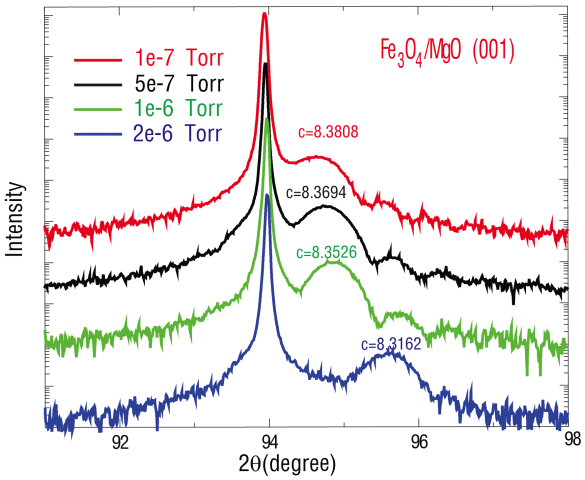

Figure 1. X-ray diffraction patterns of iron oxides on MgO(001) substrates prepared under various ozone pressures.

2. Surface reconstruction of Fe_3O_4 on MgO substrate

Figure S2 shows typical RHEED patterns, and associated line profiles, obtained for a MgO (001) substrate (top) and a 60-unit-cell-thick Fe_3O_4 film (bottom) along [100] and [110] directions. The pattern displays no evidence of 3-dimensional spots and is consistent with layer-by-layer growth. The RHEED pattern on Fe_3O_4 along [100] is consistent with a surface lattice parameter that is twice that of MgO. Along the [110] direction (Fig. S2(c)), quarter-order streaks are observed relative to the MgO substrate. This indicates a four-fold increase in the repeat distance on the Fe_3O_4 surface along [110] relative to MgO (001), consistent with a $(\sqrt{2}\times\sqrt{2})$ R45° reconstruction. The occurrence of this surface reconstruction has been reported in many studies in the past decades.[2,3] The absence of these reconstruction features has been confirmed in a γ-Fe_2O_3 (001) film grown on MgO substrate in presence of higher ozone pressure, where a (2x2) surface structure relative to the substrate and half order streaks in RHEED pattern along [110] were observed (not shown here). By these means, the growth condition for obtaining the magnetite phase has been determined.

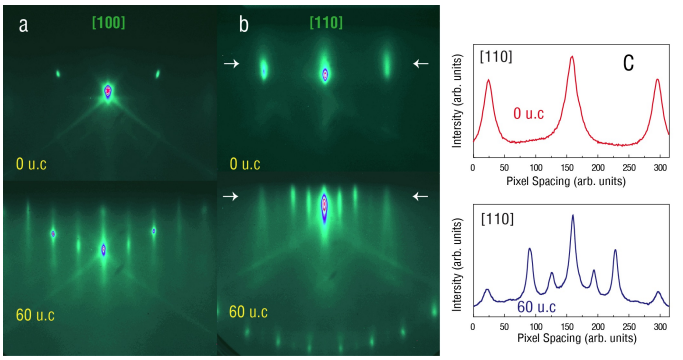

Figure S2. (a,b) RHEED patterns of MgO (001) substrate and epitaxial Fe_3O_4 film, with primary beam alignment along [100] and [110]. (c) Intensity line profile of RHEED pattern along [110] direction.

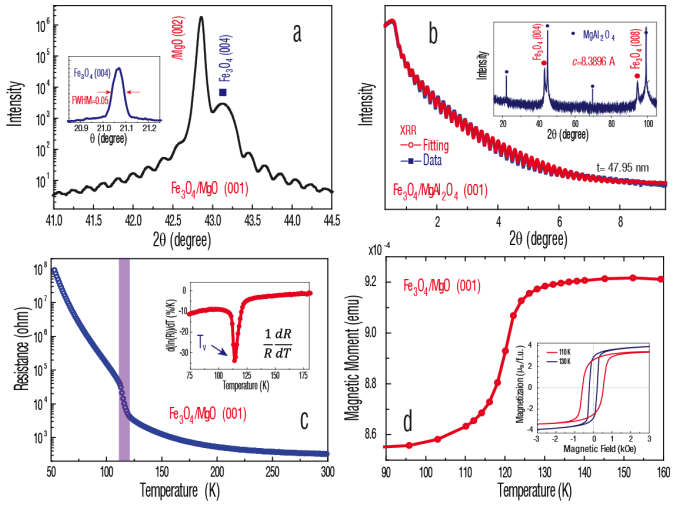

Figure S3. (a) X-ray diffraction profile of Fe_3O_4/MgO at peak position of MgO (002) with Kiessig fringes. Inset is the rocking curve of Fe_3O_4 film measured at (004) Fe_3O_4 peak. (b) X-ray reflectivity spectrum (blue) of $Fe_3O_4/MgAl_2O_4$ (001) and its fitting curve (red). Inset is the x-ray diffraction spectrum. (c,d) Temperature dependence of resistance and magnetization in Fe_3O_4/MgO (001), indicating that the Verwey transition occurred at 118 K.

3. Characterization of epitaxial Fe_3O_4 films grown on MgO, $MgAl_2O_4$, PMN-PT(001), and PMN-PT(011)

Figure S3(a) shows (004) diffraction peaks of Fe_3O_4 near the MgO (002) substrate peak. The *c*-axis parameter is 8.381 Å, consistent with an epitaxially tensile strained Fe_3O_4 film on the MgO substrate. A high degree of out-of-plane crystallinity was determined by the full width at half maximum (FWHM) of the rocking curve of 0.05° at the (004) peak position as shown in the inset. A φ-scan of the (101) peaks (not shown) verified the fourfold symmetry of the film matching that of the MgO substrate. Kiessig interference fringe oscillations indicate an atomically smooth surface and interface with MgO. Epitaxial Fe_3O_4 films were also deposited on $MgAl_2O_4$ (001) substrates at the same growth condition. Atomic layer control of synthesis and pure magnetite phase were demonstrated in our structural characterization by x-ray reflectivity and x-ray diffraction as shown in Fig. S3(b). Strong reflectivity oscillations observed up to $2\theta = 8^0$ indicates an atomically smooth surface. The x-ray reflectivity spectrum was fitted by Parratt's dynamical formalism (red line). The film thickness and surface roughness were determined to be 47.95 nm and less than 0.2 nm respectively. Electric transport and magnetic properties of epitaxial Fe_3O_4 films on MgO (001) were measured using four point technique and a superconducting quantum interference device (SQUID). Resistivity as a function of temperature (Fig. S3(c)) exhibits a sharp resistance increase upon lowering the temperature with an onset around T = 125 K, indicating metal-insulator Verwey transition. The temperature dependence of the relative resistance change (d(ln(*R*))/d*T*) shows the sharpest increase at 118 K (upper-corner insets). Figure S3(d) shows the magnetic moment as the function of temperature, indicating an decrease in magnetic moment as the temperature dropped from 130 K to 115 K. The presence of a sharp Verwey transition evidenced by resistivity and magnetization measurements and the high crystalline quality sets an upper limit of δ=0.002 on the off-stoichiometry in $Fe_{3(1-\delta)}O_4$.[4]

Epitaxial Fe_3O_4 films were also deposited on single crystal (001) and (011) oriented PMN-PT substrates with optimized growth conditions. Figure S4 shows the structural, electric and magnetic properties of epitaxial Fe_3O_4 films grown on (001) and (011) PMN-PT substrates. The single crystal structure was verified through x-ray diffraction measurement (Fig. S4(a)). Wide-angle θ-2θ scans exhibit well-oriented Fe_3O_4 peaks near the substrate peaks without secondary phases. The out-of-plane lattice parameter of the Fe_3O_4 films are determined to be 0.838 nm and 0.592 nm for (001) and (011) orientation respectively, which are close to bulk values,[1] suggesting the films are completely relaxed. The thickness of films were determined to be 55 nm for both Fe_3O_4 (001) and Fe_3O_4 (011) by fitting to x-ray reflectivity spectra. A streaky RHEED pattern on the Fe_3O_4 (001) film was observed during the MBE growth up to a thickness of 55 nm as shown in the inset, indicating a nearly atomically smooth surface.

The substrate's domain structure was imaged by atomic force microscopy (AFM) as shown in Fig. S4(b). PMN-PT has rhombohedral structure with a=4.02 A and α=89.9°. At room temperature, the ferroelectric polarization (***P***) points along the <111> body diagonals of the pseudocubic cell. Therefore, the surface of PMN-PT shows structural kinks at ferroelectric domain walls where the orientation of ***P*** changes by less than 180°. Within a single substrate domain, the root mean square (rms) roughness is less than 0.3 nm. However, during the growth of Fe_3O_4 at 300 °C, the PMN-PT substrate is in the high symmetry cubic phase and shows an intense specular spot in the RHEED pattern, indicating an atomically smooth surface.

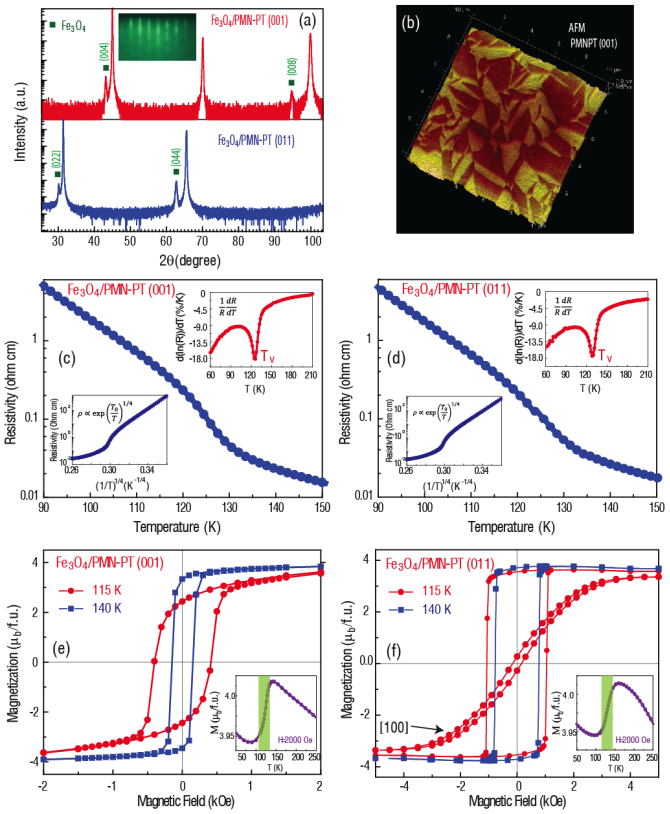

Figure S4. Structural and property characterization of epitaxial Fe_3O_4/PMN-PT heterostructures (a) X-ray diffraction spectra of epitaxial Fe_3O_4 films on (001) and (011) oriented PMN-PT substrates. Inset is the RHEED pattern for 55 nm Fe_3O_4 film on PMN-PT (001). (b) AFM image of PMN-PT (001). (c,d) Resistivity as a function of temperature for Fe_3O_4/PMN-PT(001) and Fe_3O_4/PMN-PT(011). (e,f) In-plane magnetic hysteresis loops near T_V at various temperatures for both (001) and (011) oriented Fe_3O_4 films. Insets show temperature dependence of the magnetic moment.

Electric transport and magnetic properties of epitaxial Fe_3O_4 films on PMN-PT (001) and PMN-PT (011) were measured using a four-probe technique and a superconducting quantum interference device (SQUID) magnetometer, respectively. The temperature dependence of resistivity as shown in Fig. 4S(c) and 4S(d) exhibits an abrupt change at T=125 K, indicating a Verwey transition. The relative resistance change as a function of temperature ($\frac{d(lnR)}{dT} = \frac{1dR}{RdT}$) confirmed the transition with a rapid resistance increase at 125 K (top corner insets). Below T_V, the resistance increases as $R \sim \exp\left(\frac{T_0}{T}\right)^{\alpha}$ (α is extracted to be 0.242 which is lose to 1/4.), which is consistent with variable range hopping in three dimensions (bottom-corner insets). T_0 is fitted to be 1.2×10^8 K in a small low temperature range within the resistivity change less than 2 orders of magnitude and is close to the reported values.[2, 3] Figures S4(e) and S4(f) show in-plane *M-H* loops for both Fe_3O_4 (001) and Fe_3O_4 (011) films around the Verwey transition. A distinct increase in magnetocrystalline anisotropy (determined from *M-H* loop measurements) was observed as *T* was lowered from 140 K to 115 K. This is also evident in the *T* dependence of the in-plane *M* at an intermediate field of 2000 Oe (insets). The increase in *M* upon increasing T from 110 K - 130 K for both (001) and (011) oriented Fe_3O_4 films is characteristic of the Verwey transition. The (011)-oriented Fe_3O_4 film exhibited in-plane magnetocrystalline anisotropy with the magnetic easy axis along the in-plane $[01\bar{1}]$ direction and hard axis along [100] direction, consistent with other reports of epitaxial Fe_3O_4 (011) film on MgO substrates.[4] The coercive fields in both (001) and (011) oriented Fe_3O_4 are changed as the temperature drops through the Verwey temperature (T_V) due to a magnetic anisotropy change induced by the structural transition.

4. Effects of induced by hydrostatic pressure and biaxial stress on Verwey temprature

In order to compare with the previous reports, where the T_V was suppressed by applying hydrostatic pressure on single crystal magnetite, the volume changes induced by biaxial piezo stress in magnetite thin film and by hydrostatic pressure in magnetite bulk were calculated. Given Hooke's Law in three dimensions, the strain ε can be expressed as:

$$\begin{cases} \varepsilon_x = \frac{1}{E}[\sigma_x - \nu(\sigma_y+\sigma_z)] \\ \varepsilon_y = \frac{1}{E}[\sigma_y - \nu(\sigma_x+\sigma_z)] \\ \varepsilon_z = \frac{1}{E}[\sigma_z - \nu(\sigma_x+\sigma_y)] \end{cases} \quad \ldots\ldots(1)$$

Where, σ is the stress due to piezo force or hydrostatic pressure; ν is Poisson's ratio for Fe_3O_4, equal to 0.26; *E* is Young's modulus of $2.3\times10^{12} dyne/cm^2$. The total volume change is $\frac{\Delta V}{V} = (1+\varepsilon_x)(1+\varepsilon_y)(1+\varepsilon_z) - 1$.

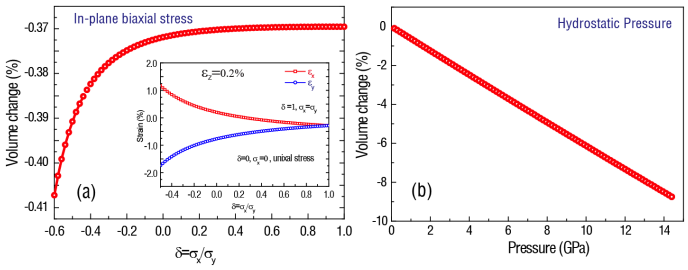

Figure S5. (a) The volume change of epitaxial Fe_3O_4 films induced by the in-plane biaxial stress. Inset is the calculated in-plane strain. (b) The volume change as a function of hydrostatic pressure in bulk Fe_3O_4

Considering in-plane biaxial stress produced by applying an electric field to the PMN-PT substrate, where the out-of-plane stress σ_z is zero, the strain in Eq. (1) can be rewritten as:

$$\begin{cases} \varepsilon_x = \dfrac{\nu-\delta}{\nu(1+\delta)}\varepsilon_z \\ \varepsilon_y = -\dfrac{1-\delta\nu}{\nu(1+\delta)}\varepsilon_z \end{cases}$$

Here, ε_z was determined to be 0.2% by *in situ* x-ray measurement; $\delta = \frac{\varepsilon_x}{\varepsilon_y}$, and $\delta = 0,1$ represent uniaxial and

isotropic biaxial piezo-strains respectively. Figure S5(a) shows the volume change and strain as a function of δ, implying a volume change of 0.3% - 0.4% induced by piezo-stress. Within this volume change, piezo-strain induced suppression of the Verwey temperature by 5-8 K was realized.

When magnetite bulk crystals are subjected to hydrostatic pressure, the strains along different directions are nominally equal and may be expressed as $\varepsilon_x = \varepsilon_y = \varepsilon_z = \frac{1}{E}\sigma(1-2\nu)$. The observed volume change as a function of hydrostatic pressure from a previous study is shown in Fig. S5(b) (From Ref. [5]). To achieve an equivalent suppression of the Verwey temperature by 5-8 K, a volume change of 3% was required, which is one order of magnitude higher than the volume change induced by piezo stress. Thus, in-plane piezo-strain is a more effective way to suppress the Verwey transition compared to hydrostatic pressure.

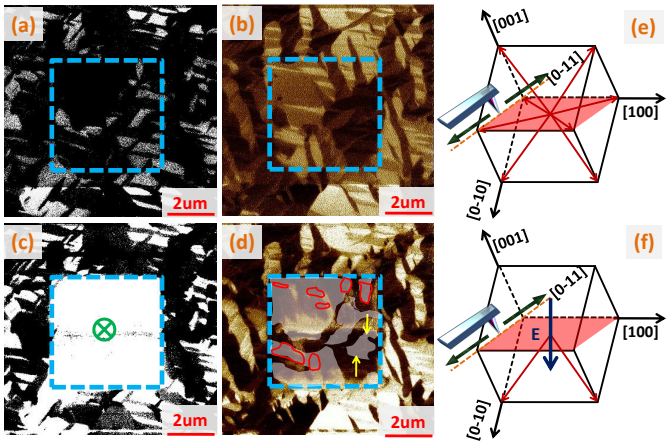

Figure S6. Ferroelastic switching path in (011) oriented PMN-PT crystals at nanoscale. (a) and (c) are the out-of-plane PFM phase images in the unpoled and poled states, respectively. (b) and (d) show that in-plane projections of the polarization along <100>, perpendicular to the cantilever, exist in both poled and unpoled states. (e) and (f) show the different configurations of the polarization vectors in unpoled state and poled states, respectively.

6. Electric-field-induced ferroelastic switching in PMN-PT(011) probed by Scanning Probe Microscope

To understand the microscopic origin of the non-volatile control of the Verwey transition, ferroelectric polarization switching in (011) oriented PMN-PT at nanoscale has been studied. We used piezoresponse force microscopy (PFM) to image the domain structure in different poling states.

Scaning along <0-11>: To complement the measurements, the cantilever was scanned along the <0-11> direction (the green arrow), which would make the LPFM phase images sensitive to the in-plane polarization in the <100> directions. Figures S6(a) and S6(b) are the out-of-plane and in-plane domain images of the PMN-PT (011) crystal as-grown state. The polarization vectors in a rhombohedral structure (Fig. S6(e)) point along the body diagonals of the pseudocubic cell at room temperature, and domain contrast for both in-plane and out-of-plane polarization directions are clearly visible. After a probe switching by a DC voltage of +10 V on the tip, all the polarization vectors rotate downward in the poled area (blue box) [out-of-plane PFM image in Fig.S6(c)]. In this poled state, domains of in-plane polarization components along <100>, perpendicular to the scanning direction, are clearly visible. This is in contrast to the scan along the <100> direction (Fig. 3 main text), where in-plane domains of polarization parallel to <0-11> are not visible in the poled state. This is because the poled out-of-plane polarization state has projections along <100> but none along <0-11>.

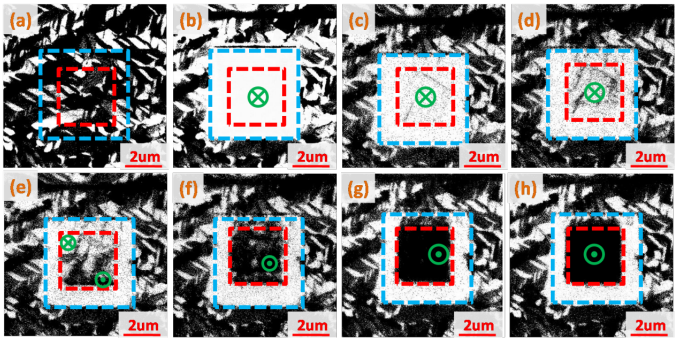

Figure S7. Out-of-plane polarization components of the different poling states. (a) as grown state, (b) +10v dc switching voltage in blue box, (c) to (h) -3v,-4v,-5v,-6v,-7v,-8v dc switching voltage in red box, respectively.

Switching Dynamics for scans along <100>: The switching dynamics during the poling process has been investigated by a probe-bias-dependent analysis for scans along <100>, which are sensitive to in-plane polarization along <0-11>. Figure S7 shows the detailed probe-bias-dependent out-of-plane domain switching dynamics: The out-of-plane polarization components rotate gradually from downward (starting state) to upward (final state) with the increasing negative dc voltage from -3v to -8v, respectively. Figure S8 shows the detailed probe-bias-dependent in-plane domain switching dynamics: The in-plane projections of the starting and final states [Figures S8(b) and (h)] are parallel to the cantilever indicating the polarization vectors are completely in the out-of-plane directions. In the intermediate states [Figures S8(c) to S8(g)], the in-plane projections perpendicular to the cantilever (i.e polarizations along <0-11>) are clearly visible (light and dark brown colors in red box), which is due to a pure in-plane polarization domains.

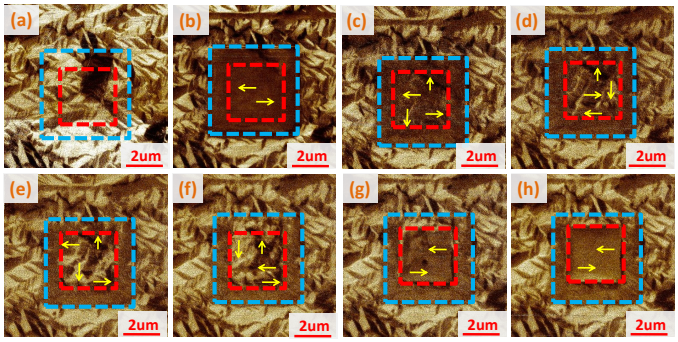

Figure S8. In-plane polarization components of the different poling states, scanning along <100> (same as Fig. 3 in paper). (a) As grown state, (b) +10v dc switching voltage in blue box, (c) to (h) -3v,-4v,-5v,-6v,-7v,-8v dc switching voltage in red box, respectively. Yellow arrows represent the directions of in-plane polarization projections.

Figure S9 shows the fraction of the intermediate switching state as a function of probe voltage. The proportion of the in-plane projection along <0-11> (perpendicular to the cantilever) increases up to 70% and then reduces with increasing negative switching voltage.

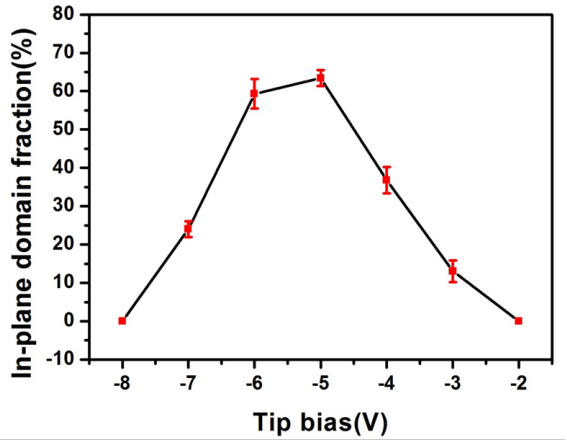

Figure S9. The fraction of the in-plane projection perpendicular to the cantilever in the poling process.

[1] F. Walz, Journal of Physics: Condensed Matter 2002, 14, R285.
[2] G. K. Rozenberg, G. R. Hearne, M. P. Pasternak, P. A. Metcalf, J. M. Honig, Physical Review B 1996, 53, 6482.
[3] G. Q. Gong, A. Gupta, G. Xiao, W. Qian, V. P. Dravid, Physical Review B 1997, 56, 5096.
[4] R. G. S. Sofin, S. K. Arora, I. V. Shvets, Physical Review B 2011, 83, 134436.